Electronic excitation in H^+-C_{60} collisions: Evaporation and ionization

J. Opitz, H. Lebius, S. Tomita, and B. A. Huber*
Département de Recherche Fondamentale sur la Matière Condensée, SI2A, CEA-Grenoble, 17 rue des Martyrs, F-38054 Grenoble Cedex 9, France

P. Moretto Capelle, D. Bordenave Montesquieu, and A. Bordenave Montesquieu
Laboratoire CAR-IRSAMC, Université Paul Sabatier, 118 Route de Narbonne, F-31062 Toulouse, France

A. Reinköster, U. Werner, and H. O. Lutz
Fakultät für Physik, Universität Bielefeld, D-33501 Bielefeld, Germany

A. Niehaus and M. Benndorf
Debye Institute, Utrecht University, Princetonplein 5, 3508 TA Utrecht, The Netherlands

K. Haghighat, H. T. Schmidt, and H. Cederquist
Atomic Physics, Stockholm University, Frescativägen 24, S-10405 Stockholm, Sweden
(Received 23 February 2000; published 13 July 2000)

We have studied energy transfer, fragmentation, and ionization in collisions between protons and C_{60} molecules. The collision energy is varied between 1 and 300 keV and we thus cover a velocity range from 0.2 to 3.5 atomic units. The distributions of intact and fragmented C_{60} ions have been measured by means of time-of-flight mass spectrometry using pulsed beams or emitted electrons to clock the collision events. The processes leading to multiple ionization and evaporation of neutral dimers are analyzed as functions of the projectile velocity. In contrast to recent findings for He^+-C_{60} collisions by Schlathölter *et al.*, our results show that the cross sections for ionization and evaporation first increase with velocity, have maxima at around 1–2 a.u., and decrease again for higher velocities. This velocity dependence closely resembles the one for the electronic stopping power indicating that electronic excitations are the main means of energy transfer to C_{60} and that this energy is rapidly distributed among the vibrational degrees of freedom. This conclusion is supported by Monte Carlo calculations of nuclear and electronic energy loss for protons passing through and closely outside the C_{60} cage.

PACS number(s): 34.50.Bw, 34.50.Ez, 34.50.Gb, 34.70.+e

I. INTRODUCTION

Electronic and vibrational excitation of finite many-body systems is an active field of current research. In particular, the importance of differently activated decay processes, such as electron emission, fragmentation, or evaporation of neutral particles, and the energy sharing among the decay channels including the transfer of electronic excitation energy towards vibrational excitation modes, are not well understood. Some of these aspects have been studied recently in collisions between C_{60} fullerenes and different particles such as photons [1–4], electrons [5–7], atoms [8], and singly [9,10] or multiply charged ions [10–19].

In the present contribution we will discuss the degree of vibrational excitation and the degree of ionization when a singly charged ion (H^+) interacts with a C_{60} fullerene. For such a collision, we expect that single-electron capture without large excitations of the system dominates at large impact parameters and low velocities ($v<1$ a.u.). The critical over-the-barrier distance for single-electron transfer from C_{60}, modeled as an infinitely conducting sphere [11,19], to a singly charged ion is 14.8 a.u. A comparison of this value with the radius of the C_{60} molecule ($\sim$7 a.u.) makes it clear that a substantial part of the ionizing events is due to collisions, where the proton penetrates the C_{60} cage. Referring to the energy loss of H^+ ions in graphite, we expect that the electronic stopping power dominates the nuclear stopping power, particularly at high collision velocities. Therefore, electronic excitation should dominate direct vibrational excitation in the presented velocity range.

In recent publications [9,20], it was shown for He^+-C_{60} collisions that ionization and multifragmentation of C_{60} molecules on the one hand and the evaporation of C_2 dimers on the other hand have different velocity dependences. In the former case, the signal increases strongly with velocity ($v=0.1-1$ a.u.), whereas it decreases strongly in the latter case. This clearly proves that direct vibrational excitation leads preferentially to evaporation, whereas electronic excitation causes ionization and multiple fragmentation of C_{60} for He^+ projectiles [9,20]. In the present work we show that the velocity dependence for evaporative fragmentation of C_2 molecules is similar to that of the electronic energy loss for H^+-C_{60} collisions. In a way, this is in contrast to results at similar velocities for He^+-C_{60}, where a transfer of electronic excitation energy to vibrational modes seemed to be of little importance. Studies at high velocities (>1 a.u.) with heavy ions in charge states 1 to 3 [21] also show that fragmentation

*Corresponding author.

is predominantly induced by electronic excitation.

In the following we will briefly describe the main features of the experiments and discuss the Monte Carlo method applied to calculate the electronic and nuclear energy losses before presenting and discussing the experimental results.

II. EXPERIMENTAL TECHNIQUE

The experiments have been performed in three laboratories using different ion sources and accelerators but similar experimental techniques. It was thus possible to cover wide energy and velocity ranges. The basic principle of the different experiments is rather similar. A beam of hydrogen ions is crossed with an effusive beam of C_{60} molecules. This beam is emerging from a heated oven which is held at a temperature of about 500 °C and contains a high-purity C_{60} powder. The interaction zone is a part of the extraction zone of a linear time-of-flight mass spectrometer of the Wiley-McLaren type [22,23]. Accelerated recoil ions pass a drift region with lengths varying between 10 cm and 1 m for the different devices, and are detected by a channelplate detector with or without position sensitivity.

Different modes of operation have been applied. Either the ion beam and (or) the extraction voltage applied to the mass spectrometer have been pulsed with frequencies of typically a few kHz. In this case, the extraction pulse served as a start signal for the time-of-flight measurement and the stop signal was provided by secondary ions having passed the flight path. Both signals are treated with a ''multihit'' time-to-digital converter followed by a workstation as an analyzing device. In this way, all produced ions and fragments are detected, yielding what we will refer to as ''inclusive'' time-of-flight (TOF) spectra. They are completely independent of the charge state, the scattering angle, and the energy loss (or gain) of the outgoing projectile.

Some of the present experiments have been performed with continuous beam operation and a continuous electric field was applied to the extraction region. In this case, electrons which are emitted during the collision process are accelerated to the opposite side of the ion TOF system and can be used as a start signal for the ion TOF measurement. Under these conditions, the measurement is sensitive only to events where free electrons are produced and, therefore, contributions from pure electron capture are not detected. In Fig. 1, inclusive spectra of fullerene ions and fragments are compared with spectra, where free electrons have been used as a start signal of the TOF measurement. At low collision energies (5 keV) the intensity of singly charged ions is strongly suppressed when the start is provided by the electrons. Evidently, C_{60}^{+} ions are mainly formed by pure single-electron capture, while C_{60}^{2+} and C_{60}^{3+} are often produced together with free electrons at 5 keV. However, at higher velocities direct ionization becomes dominant, and capture is further limited by dynamic effects [24]. Thus, the difference between the two spectra at 100 keV is not significant.

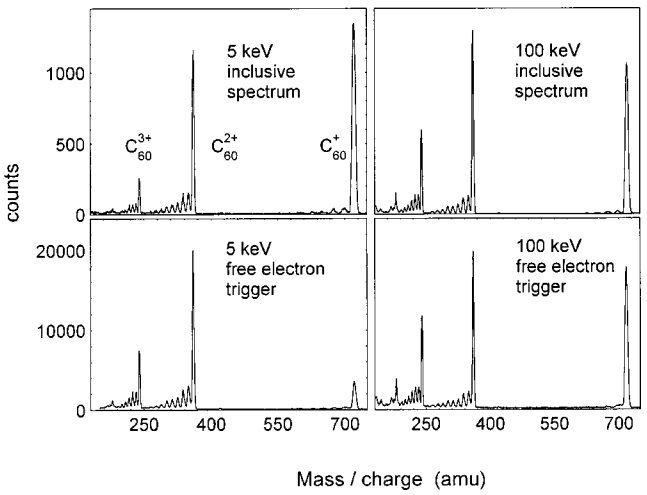

FIG. 1. Time-of-flight mass spectra of intact and fragmented C_{60} ions produced in H^{+}-C_{60} collisions at 5 keV (left column) and 100 keV (right column). Upper part, inclusive spectra; lower part, spectra triggered by free electrons (cf. text).

With continuous beams, a delayed start signal for the time-of-flight measurement can also be obtained by the projectile, which has to be charge-state-selected after the collision. In fact, the experimental setup in Grenoble allows us to measure the charge state, the kinetic energy, and the scattering angle of the projectile when it remains charged after the collision. In the case of neutralized projectiles, only the scattering angle can be measured.

The main features of the different experiments are summarized in Table I. The second column shows that the different experiments allow for a good overlap in the collision energy covering a range between 1 and 300 keV. Whereas column 3 indicates the possible operation modes, column 4 gives the voltages which have been used to postaccelerate the fullerene ions before they are detected. These values determine the detection efficiency for ions in different charge states. Although the secondary electron yield due to potential emission has been shown to be independent of the fullerene charge state [25], the different kinetic energies will result in different signal heights. An analysis of the spectra obtained with 6 and 30 kV showed that in the first case the intensity of

TABLE I. Details of the different experiments used for this study.

Experiment	Energy range (keV)	Operation mode	Postacceleration for recoil ions (kV)	Start signal
Grenoble I	1–3	pulsed or continuous	6	pulse or projectile
Grenoble II	2–20	pulsed	30	pulse
Toulouse	5–150	pulsed or continuous	4	pulse or electron
Bielefeld	100–300	continuous	5.5	electron

singly and doubly charged fullerene ions has to be corrected by 22% and 14%, respectively. More details on the different experiments are given in Refs. [17,26–28].

III. MONTE CARLO CALCULATIONS OF THE PROJECTILE ENERGY LOSS IN H^+-C_{60} COLLISIONS

We have calculated the projectile energy loss and angular scattering for the present H^+-C_{60} collisions using a newly developed Monte Carlo method [19]. The electronic energy loss is calculated by means of the Firsov model [29], which is based on the concept of electron transfer between two colliding atoms and the acceleration of electrons from one frame of reference to the other. As one electron is transferred from a target atom at rest to a projectile atom with initial velocity v_0, the latter is slowed down by an amount $(m_{\mathrm{el}}/M)v_0$ and its kinetic energy decreases [29] (m_{el} and M being the masses of the electron and the projectile). This concept is of course only valid in the velocity range at which an electron released from the target is attached to the projectile, setting an upper limit of about 20 keV for H^+-C_{60} collisions. At somewhat higher energies, impact ionization begins to be important and Coulomb scattering on quasifree electrons is better at describing the electronic part of the energy loss of the projectile. This feature is not included in the present Monte Carlo calculations. Therefore, the electronic energy losses are only valid for proton energies below 20 keV. However, it is worthwhile to note here that the velocity dependence of the electronic energy loss at higher velocities is expected to be the same as that of the nuclear energy loss, i.e., inversely proportional to the velocity. The nuclear, or elastic, energy loss and the associated angular scattering is calculated by using the Molière potential [30] to describe the effective interactions between the heavy particles. This picture is valid for the whole present kinetic energy range (1–300 keV).

The Monte Carlo program uses four random numbers for each simulated ion trajectory, one to select the impact parameter with respect to the center of C_{60} ($b_{C_{60}}$) and three to rotate the molecule randomly. For each randomly selected trajectory and molecular orientation, we calculate the nuclear and electronic energy losses and the projectile angular scattering due to 60 *purely atomic* hydrogen-carbon collisions. The specific geometry of the C_{60} molecule is taken into account by positioning free, i.e., unperturbed, carbon atoms in the 60 corners of a truncated icosahedron. This randomly oriented model C_{60} molecule is then projected on a plane perpendicular to the initial direction of the projectile trajectory and 60 *atomic impact parameters* may now be defined. We sum the electronic and nuclear energy losses separately for the 60 simultaneous *atomic* collisions using the Firsov formula [29] and the Molière potential [30], respectively. Further, we calculate the scattering angle for the projectile by adding the 60 momentum vectors to the (longitudinal) momentum vector of the incoming projectile.

The present Monte Carlo program has been used earlier for comparisons with experimental results on angular scattering and energy loss in collisions of Ar^{8+} on C_{60} at 26 keV [19] and for energy loss in 100 keV Ar^{3+}-C_{60} collisions [31].

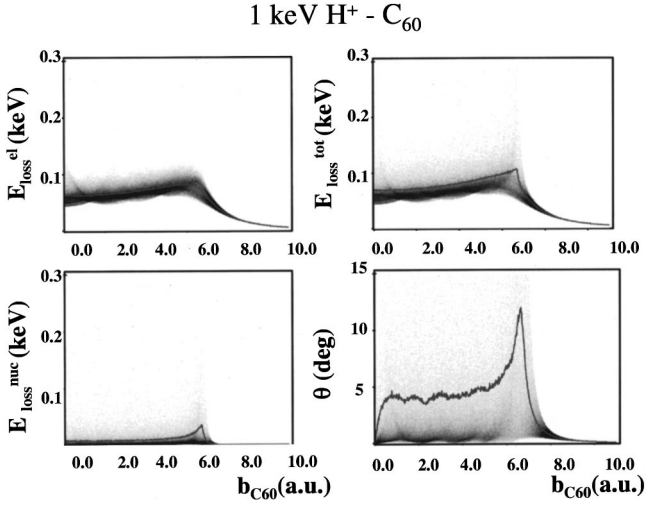

FIG. 2. Monte Carlo calculations of electronic, nuclear, and total-energy losses (denoted as $E_{\mathrm{loss}}^{\mathrm{el}}$, $E_{\mathrm{loss}}^{\mathrm{nuc}}$, and $E_{\mathrm{loss}}^{\mathrm{tot}}$, respectively) as functions of the impact parameter $b_{C_{60}}$ for 1 keV H^+-C_{60} collisions. The total-energy loss is calculated as the sum of the nuclear and electronic energy losses for each individual trajectory. The scattering angle θ, calculated from the elastic (nuclear) scattering, is also shown as a function of $b_{C_{60}}$. The full lines indicate the average values while the points give the results for individual trajectories (cf. text). The densities of points are proportional to the probabilities for the corresponding resulting values of $E_{\mathrm{loss}}^{\mathrm{el}}$, $E_{\mathrm{loss}}^{\mathrm{nuc}}$, $E_{\mathrm{loss}}^{\mathrm{tot}}$, and θ.

The comparisons were made for low charge states of the outgoing projectiles—the signature of close collisions—and rather good agreement with the experimental results was established [19]. We have also calculated the nuclear and electronic energy losses for 1–80 keV He^+-C_{60} collisions in order to compare the results with the calculations by Schlathölter *et al.* [9]. Our calculations basically confirm the ones reported in Ref. [9]. This point is most important since the comparison between the present experimental and theoretical results on H^+-C_{60} collisions lead us to a conclusion which differs from the one by Schlathölter *et al.* [9].

In Fig. 2, we show results for electronic, nuclear, and total-energy loss and projectile scattering angles as functions of $b_{C_{60}}$ for 1 keV H^+-C_{60} collisions. We have launched 3×10^6 trajectories for each plot. The densities of points are proportional to the number of trajectories giving results within small finite intervals of energy loss and scattering angle in the respective figures. We note that the same value of $b_{C_{60}}$ may lead to different results, which is due to the many possible orientations of the C_{60} molecule which in turn may or may not favor close collisions with individual carbon atoms. The full curves show the mean values and we note that these are not representative for the typical events for the nuclear energy loss and scattering. The reason for this is that a few trajectories give very large values for θ and $E_{\mathrm{loss}}^{\mathrm{nuc}}$ which strongly affect the corresponding mean values. The mean values have their maxima for trajectories passing close to the surface of the C_{60} cage, i.e., for $b_{C_{60}}$ close to 6.7 a.u., in all

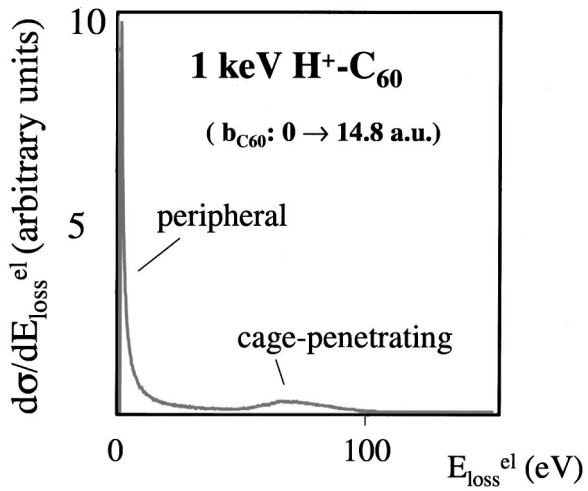

FIG. 3. The distribution of the electronic energy loss of the projectile in 1 keV H^+-C_{60} collisions. These data are obtained by averaging over the Monte Carlo results for the electronic energy loss in the impact parameter range 0–14.8 a.u. The two maxima are due to peripheral and cage-penetrating collisions (cf. text).

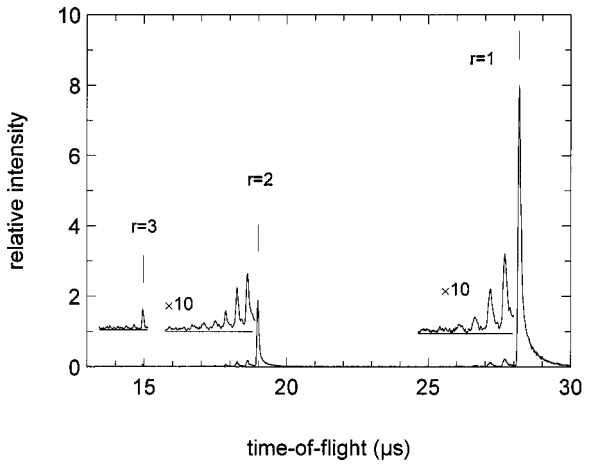

FIG. 4. Inclusive time-of-flight mass spectrum, recorded with a pulsed extraction voltage and a continuous ion beam, for 1 keV H^+-C_{60} collisions. The positions for the intact $C_{60}{}^{r+}$ molecules are indicated by $r=1$, 2, and 3. The evaporation sequences are $C_{60-2m}{}^{r+}$, where m denotes the number of emitted C_2 molecules.

four figures. By comparing the absolute values for the electronic and nuclear energy loss in Fig. 2, we may conclude that the former dominates the latter one even for these low velocities. This can also be seen in the strong resemblance of $E_{\mathrm{loss}}^{\mathrm{el}}$ and $E_{\mathrm{loss}}^{\mathrm{tot}}$ as shown in Fig. 2.

In Fig. 3, we show the Monte Carlo results for $d\sigma/dE_{\mathrm{loss}}^{\mathrm{el}}$ for 1 keV H^+-C_{60} collisions for the impact parameter interval $b_{C_{60}}=0-14.8$ a.u., where the upper limit was deduced from the classical over-the-barrier criterion for single-electron capture to the projectile assuming that C_{60} can be modeled as an infinitely conducting sphere [19]. The first maximum, at low $E_{\mathrm{loss}}^{\mathrm{el}}$, is due to trajectories outside the cage whereas the second maximum close to $E_{\mathrm{loss}}^{\mathrm{el}}=60$ eV is due to penetrating trajectories. The minimum in $d\sigma/dE_{\mathrm{loss}}^{\mathrm{el}}$ is related to the passage just outside the cage where $E_{\mathrm{loss}}^{\mathrm{el}}$ changes rapidly as a function of $b_{C_{60}}$ (cf. Fig. 2). For penetrating collisions $E_{\mathrm{loss}}^{\mathrm{el}}$ changes slowly with $b_{C_{60}}$ and the width of the peak at 60 eV reflects the spread in $E_{\mathrm{loss}}^{\mathrm{el}}$.

IV. EXPERIMENTAL RESULTS

In Fig. 4 we show an inclusive time-of-flight spectrum for 1 keV H^+-C_{60} collisions. The dominant peaks are due to ionized and intact $C_{60}{}^{r+}$ ions with intensities decreasing with increasing recoil charge $r=1-3$. $r=3$ is the maximum charge. The asymmetric peak form is due to the fact that the spectra have been recorded with a continuous ion beam and a pulsed extraction voltage. The signals of intact fullerene ions are accompanied by evaporation sequences, which are due to the thermally activated evaporation of neutral C_2 molecules. Depending on the charge state of the parent $C_{60}{}^{r+}$ ion, up to seven C_2 units have been emitted indicating that large amounts of energy have been deposited in the vibrational modes of the ionized fullerenes.

In Fig. 5 we show mass spectra for H^+-C_{60} collisions at 2, 10, 60, and 200 keV. The former three are inclusive spectra while the last one, recorded at Bielefeld, is measured with the free-electron trigger. We showed in Sec. II (cf. Fig. 1) that the difference between inclusive and electron-trigger spectra was insignificant for high velocities. Thus, we may compare all four spectra of Fig. 5 directly and we note that the intensities of the more highly charged intact fullerenes

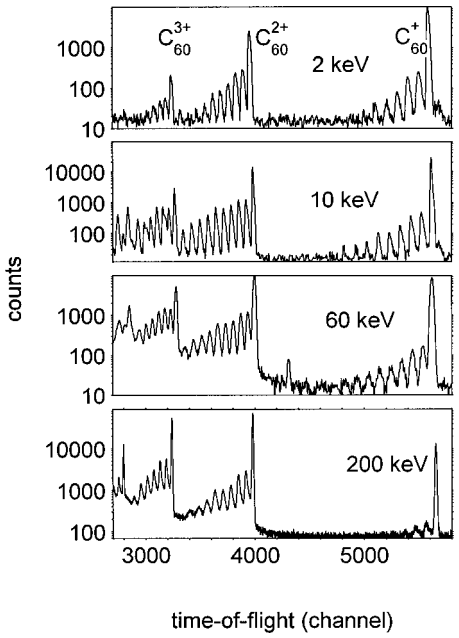

FIG. 5. Time-of-flight mass spectra measured in H^+-C_{60} collisions. The spectra at 2 and 10 keV (measured in Grenoble) and at 60 keV (measured in Toulouse) are inclusive spectra. The high-energy data at 200 keV (measured in Bielefeld) were recorded with free-electron trigger (the additional peak at 60 keV corresponds to $C_{70}{}^{2+}$ ions).

increase with velocity. The maximum charge state for the intact molecules turns out to be 5 at higher velocities (not shown in Fig. 5). For a given r, the intensity of the evaporation sequence $C_{60-2m}{}^{r+}$ and its distribution with respect to m changes with the collision energy. The total evaporation intensity in relation to the intensity of the parent $C_{60}{}^{r+}$ and the corresponding maximum m first increase with v, but decrease again at higher velocities. This indicates that C_2 evaporation is most important at velocities around 1 a.u., a behavior which resembles the expected velocity dependence for the *electronic* energy loss. In contrast, the nuclear (elastic) energy loss decreases in a monotonic fashion with velocity. This result already indicates that C_2 evaporation, induced by H^+-C_{60} collisions in the energy range 1–300 keV, is caused by initial electronic energy transfer to the molecule followed by a redistribution of this energy into the vibrational degrees of freedom.

V. DISCUSSION

A. Evaporation and electronic excitation

Information about the internal energy stored in the vibrational modes of the fullerene ion can be obtained from the intensity distribution of $C_{60-2m}{}^{r+}$ ions in the measured spectra. In the present case, these ions are predominantly formed by the sequential emission of neutral C_2 molecules. Only for higher charge states ($r \geqslant 3$) does the emission of charged small carbon clusters become competitive and has to be taken into account [16]. In the following, we will neglect contributions from these fission processes.

The variation with m, the number of emitted C_2 molecules, as well as the relative intensity with respect to the intact molecule $C_{60}{}^{q+}$ can be used to estimate the deposited energy. As defined in Ref. [9], we determine a relative ''hot'' fraction f_e^{r+} (where ''e'' stands for evaporation) for a given charge state r of the molecule. The intensity ratio is given by

$$f_e^{r+} = \sum_m I(C_{60-2m}{}^{r+}) \Big/ \left[\left(\sum_m I(C_{60-2m}{}^{r+}) \right) + I(C_{60}{}^{r+}) \right], \tag{1}$$

where $I(C_{60}{}^{r+})$ and $I(C_{60-2m}{}^{r+})$ correspond to the integrated intensities of time-of-flight peaks specified by r and by r and m, respectively. When taking the sum for $m>0$, contributions from a ''hot'' distribution which are still present in the intact molecule peak are neglected (see discussion below). The evaporation fractions f_e^{1+}, f_e^{2+}, and f_e^{3+} are shown as functions of the collision velocity in Fig. 6. At low velocities the evaporation fractions increase with v, reach a maximum slightly below or close to 1 a.u., and decrease again at higher energies. This behavior is similar for all r, but the maximum values of f_e^{r+} increase from 12% to 45% and, finally, to 70% as r increases from 1 to 3.

The evaporation data from Grenoble, Toulouse, and Bielefeld are shown in Fig. 6, and since there is good agreement between results from different laboratories in the overlapping velocity regions, we have chosen to represent all the data for a given r with a common symbol. The dashed curves

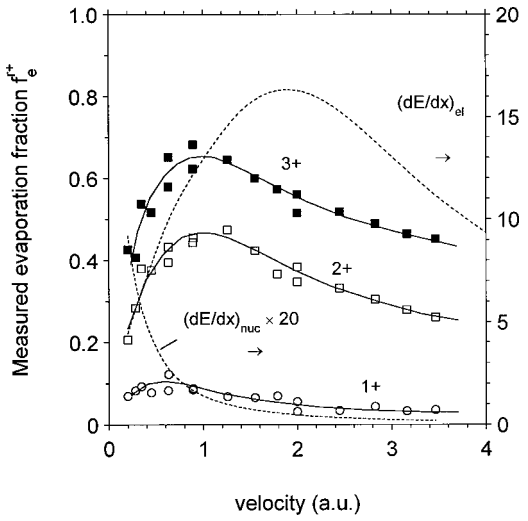

FIG. 6. Measured evaporation fractions f_e^{r+} for singly ($r=1$, open circles), doubly ($r=2$, open squares), and triply ($r=3$, full squares) charged fullerene ions as functions of the projectile velocity v (the full lines are to guide the eye only). The dashed curves represent the prediction of a TRIM calculation of the electronic and nuclear stopping power of H^+ ions in graphite [$(dE/dx)_{el}$ and $(dE/dx)_{nul}$, respectively]. The data points refer to the left-hand axis while $(dE/dx)_{el}$ and $(dE/dx)_{nuc}\times 20$ refer to the right-hand scale.

denote the electronic stopping power $(dE/dx)_{el}$ and the nuclear stopping power times 20, 20 $(dE/dx)_{nuc}$, calculated with the TRIM code [32]. The stopping power values are given by the vertical scale on the right-hand side. We immediately see that the electronic stopping power dominates by far the nuclear one in the whole present velocity region. The former is an order of magnitude larger than the latter at our lowest velocity ($v=0.2$ a.u.). Further, whereas the nuclear stopping power (lower dashed curve in Fig. 6) decreases strongly with increasing velocity, the electronic stopping power shows a similar velocity dependence to the measured fractions, indicating that evaporation and electronic excitation are closely related. This means that an appreciable amount of the electronic excitation energy which is given to the fullerene in the collision is transferred into the vibrational modes during or after the collision. Thus, for the present H^+-C_{60} collisions there is no indication of a direct excitation of the vibrational degrees of freedom by means of elastic nuclear-nuclear scattering as in the case of He^+-C_{60} collisions [9,20].

We note that the maximum of the evaporation fraction occurs for all charge states at lower velocities than the maximum of the electronic energy loss. In Fig. 7 we show the relation between the evaporation fractions, f_e^{r+}, and the electronic stopping power from the TRIM code. The evaporation increases with the electronic energy loss and reaches a saturation value before decreasing again, giving hook-shaped curves. In the hook region, low and high velocity collisions lead to the same amount of electronic energy loss but, obviously, different evaporation fractions. This result could perhaps be explained by a different distribution of the electronic

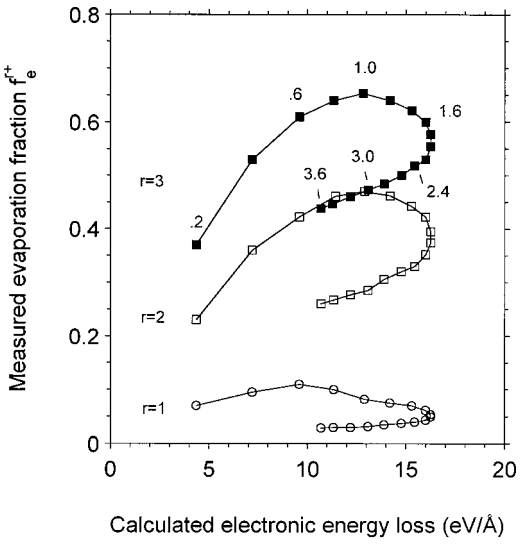

FIG. 7. Relation between the evaporation fraction f_e^{r+} for a given charge state r and the electronic stopping power calculated with the TRIM code for the H^+-graphite system. The numbers given for $r=3$ correspond to the projectile velocity in atomic units.

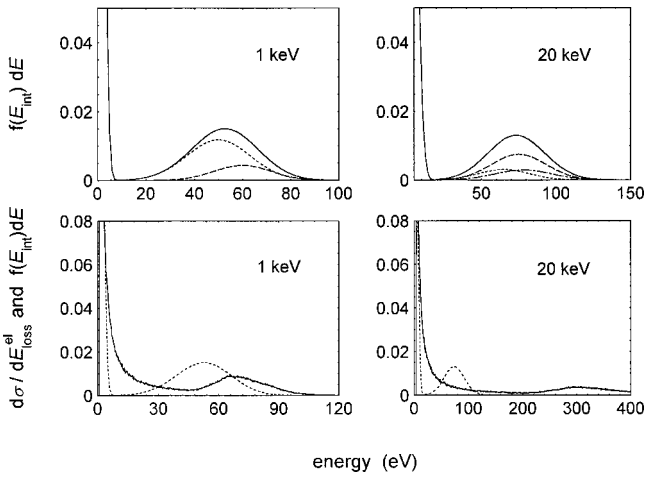

FIG. 8. Upper part: Semiempirical internal energy distributions, $f(E_{\rm int})dE$, of parent fullerene charge states $r=1$ (short dashed curves), $r=2$ (long dashed curves), and $r=3$ (short/long-dashed curve) produced in H^+-C_{60} collisions at 1 and 20 keV. The distributions are obtained from the measured intensity distributions on the $C_{60-2m}{}^{r+}$ sequences and the RRK theory describing evaporative ensembles (cf. text). The full curves show the sums of the partial, r-dependent, energy distributions. Lower part: The total internal energy distributions (dashed curves) are compared with the electronic energy losses, $d\sigma/dE_{\rm loss}^{\rm el}$, as calculated with the Monte Carlo method described in Sec. III (full curves).

excitation in C_{60} at low and high velocities. Indeed, there are important differences between these two regions. In the low-energy region, energy is transferred by the acceleration of electrons between the projectile and the target frames of reference, while Coulomb scattering on quasifree electrons becomes more important at the higher velocities. In the latter case, a non-negligible part of the deposited energy is expected to show up in the kinetic energy of ionized electrons and the part of the electronic energy loss which will be left for internal excitations of the molecule is reduced. A similar phenomenon has been found for ion collisions with thin solids and large biomolecules. In the first case, the electron yield and the secondary ion yield induced by bombarding carbon foils with He projectiles showed a strong velocity dependence [33]. In a similar way, strand breaks of the DNA molecule induced by heavy ions may create a similar ''hook'' phenomenon [34,35]. For solids, biomolecules, and C_{60} the hook feature is caused by the fact that the calculated electronic stopping power continues to increase with the collision velocity while the damage (strand breaking, fragmentation) has already reached its maximum and has started to decrease. Evidently, these damage effects which occur in solids are also observable in smaller, individual molecules, which indicates that the stopping power concept might also apply for small systems of finite size.

Assuming that the energy is statistically distributed over all degrees of freedom, we can apply the RRK theory (Rice, Ramsberger, and Kassel), which describes the behavior of an evaporative ensemble [36,37]. We express the evaporation rate $k(m,E)$ as a function of the number m of emitted C_2 molecules and the stored internal energy E by

$$k(m,E)=[(60-2m)/6](1-D_m/E)^{[3(60-2m)-7]}/t_c, \quad (2)$$

where D_m is the activation energy for the emission of the mth C_2 molecule and t_c is a time characterizing the energy transfer within the vibrational modes [38,39]. A comparison of the calculated intensity distributions with the experimental data yields an estimate of the internal energy. In our model the activation energy has been taken to be independent of the charge state of the fullerene ion: $D_m=11.9$ eV [40] [a lower value ($D_m=7.1$ eV) would lower the evaluated internal energies from 75 to 39 eV, for example, see also discussions in Refs. [1,6]].

The fit procedure showed that particularly for $r=1$ and partly for $r=2$ the internal energy has to be described by at least two Gaussian distributions in order to represent the experimental data. One of them is centered at zero energy; the relative amplitude has been normalized with the aid of our Monte Carlo calculations. The second Gaussian is centered at a higher internal energy. Fit parameters have been the amplitudes of both distributions as well as the half-width of the second one. The half-width of the ''cold'' distributions has been determined by the integrated contribution of the ''cold'' component.

In the upper part of Fig. 8 we show semiempirical internal energy distributions, $f(E_{\rm int})dE$, for different values of r. At a collision energy of 1 keV, the dominant process leads to $r=1$ by electron capture either in peripheral or in close collisions. Doubly charged fullerenes are produced only in penetrating collisions associated with higher-energy losses (about 60 eV). At 20 keV, peripheral collisions are still dominated by single capture ($r=1$: 75%; $r=2$: 25%), however a close interaction preferentially leads to double ioniza-

tion ($r=2$) followed by triple and single ''ionization.'' The stored internal energy increases with the collision velocity.

In the lower part of Fig. 8 we compare the estimated internal energies with the electronic energy losses calculated by means of the Monte Carlo method described in Sec. III for H^+-C_{60} collisions in the impact parameter interval 0–14.8 a.u. Both results [the projectile energy loss $d\sigma/dE^{\rm el}_{\rm loss}$ and the internal energy distribution $f(E_{\rm int})dE$] are in qualitative agreement at 1 keV, which seems to indicate that most of the energy that is lost by the projectile due to electronic excitation is finally transferred into vibrational modes of C_{60}. The agreement between $d\sigma/dE^{\rm el}_{\rm loss}$ and $f(E_{\rm int})dE$ is much poorer at 20 keV. The main features are still similar for the two distributions with colder parts associated with peripheral collisions and hotter parts due to penetrating collisions, but the positions in energies of the latter are rather far apart.

It should be noted that only a part of the projectile energy loss is transferred into vibrational energy causing evaporative fragmentation. The other part of the energy loss is used to ionize C_{60} and to give kinetic energy to the emitted electrons. However, the ionization part appears to be too small to explain the difference between ''hot-peak'' positions appearing in the lower right part of Fig. 8 (ionized electrons are only expected to carry away $\sim$10 eV if they are assumed to be accelerated to the projectile velocity at 20 keV). An additional and presumably more important reason for this large difference might be that the Firsov formula [29], used in our Monte Carlo calculations for the electronic energy loss, does not take into account oscillations as a function of the projectile nuclear charge. Such oscillations have been observed by Hvelpund and Fastrup [41] with rather large amplitudes thus giving substantial corrections (up to about 50%) to the predictions of the Firsov model. Since the proton data are close to a minimum in such oscillations and the amplitude decreases rather strongly with v, the electronic energy loss should vary more slowly with velocity than what is predicted by the Firsov formula for protons.

In the following we use the internal energies for close collisions, taken to be the mean values of the hot fractions of the semiempirical energy distributions $f(E_{\rm int})dE$ (c.f. Fig. 8). In Fig. 9 we show these mean values as functions of the projectile velocity v and indicate the widths of the distributions by vertical bars. These data are compared with different calculations of the *projectile energy loss*. Curves (a) and (b) show the present results of the Monte Carlo and TRIM calculations for the projectile energy loss using average atomic surface densities of (first) randomly oriented and (then) projected C_{60} molecules. This yields an atomic surface density of 15×10^{15} atoms/cm^2 (see also Ref. [31]). Curve (c) has been obtained by means of the TRIM code in which the fullerene has been replaced by two monolayers of graphite, whereby the atomic density corresponds to that of the fullerene surface (see Ref. [21]). At velocities below 0.4 a.u., curve (c) is in good agreement with quantum-mechanical results obtained recently within the nonadiabatic quantum molecular-dynamics approach (NA-QMD) by Schmidt *et al.* [42], in which the motion of the heavy particles is treated classically and the time-dependent density-functional theory is used for the electronic system. As this method is expected

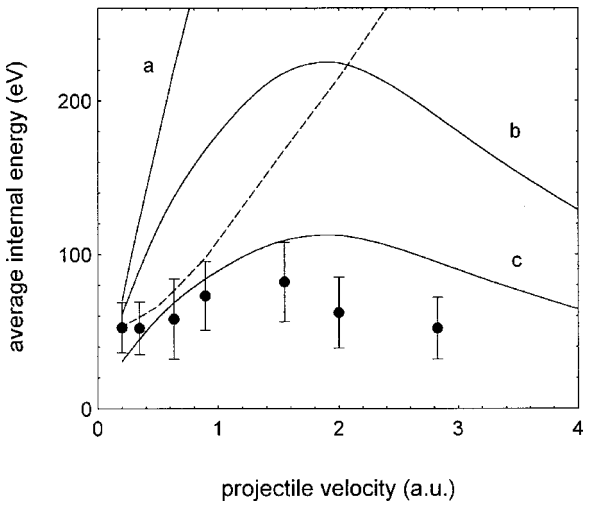

FIG. 9. Average internal energies of the ''hot fractions'' and projectile energy losses for penetrating collisions as functions of the projectile velocity v. Full circles: internal vibrational energy (determined from the evaporation series; these values include an initial thermal energy of about 12 eV); the vertical lines correspond to the widths of the estimated energy distributions. The long dashed line represents the estimated sum of the vibrational energy and the energy part which is used to ionize the fullerene ($E_{\rm vib}+E_{\rm ion}+E_{{\rm kin},e}$). The full curve (*a*) is the result of the Monte Carlo calculation describing the average energy loss for ''penetrating'' collisions. The full curves (*b*) and (*c*) are the results of TRIM calculations using different surface densities (cf. text).

to give rather precise results, in the following discussion we will consider among the curves (a), (b), and (c) the latter one as the most realistic representation of the energy loss in the whole presented velocity region.

At low velocities ($0.2<v<0.6$) the mean internal energies are nearly velocity independent; the data are in qualitative agreement with the energy losses, indicating that the major part of the electronic energy is transferred into vibrational modes. With increasing velocity, a larger amount of the energy loss should be transferred into kinetic energy of emitted electrons. Assuming that these electrons have roughly the same velocity as the projectile (simulations of H^+-Na_n collisions showed this tendency [43]), we estimate the sum of the vibrational energy $E_{\rm vib}$ and the energy to ionize ($E_{\rm ion}$) and to accelerate ($E_{\rm kin}$) the electrons (see dashed curve in Fig. 9). For this estimate the average charge state created in close collisions has been taken into account (see discussion in the next section). The estimated sum increases steeply with velocity. A comparison with curve (c) indicates that ionized electrons probably can no longer follow the fast projectile at high velocities. In this region, the fraction of the energy loss, which is transferred into vibrational modes due to electron-phonon coupling, decreases and appears to be of the order of 50%.

B. Multiple ionization

The mass spectra have been analyzed with respect to contributions from different charge states. At different velocities, the intensities of the $C_{60-2m}{}^{r+}$ peaks have been inte-

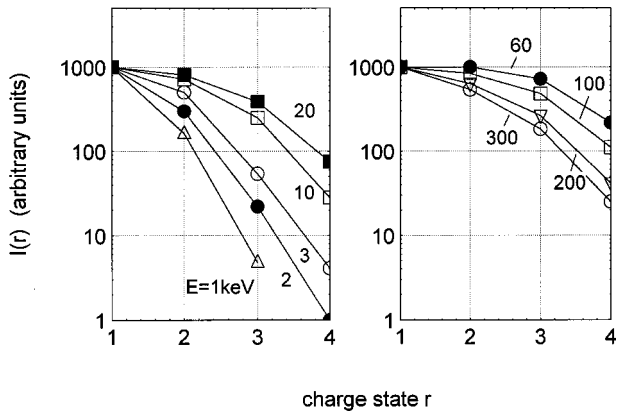

FIG. 10. Relative parent ion charge-state distributions $I(r) = \Sigma_{m=0-10} I(C_{0-2m}{}^{r+})$ are shown for projectile energies of 1, 2, 3, 10, and 20 keV (left figure) and 60, 100, 200, and 300 keV (right figure). The intensities for $r=1$ have been set to 1000 for all energies. The lines between the data points are to guide the eye.

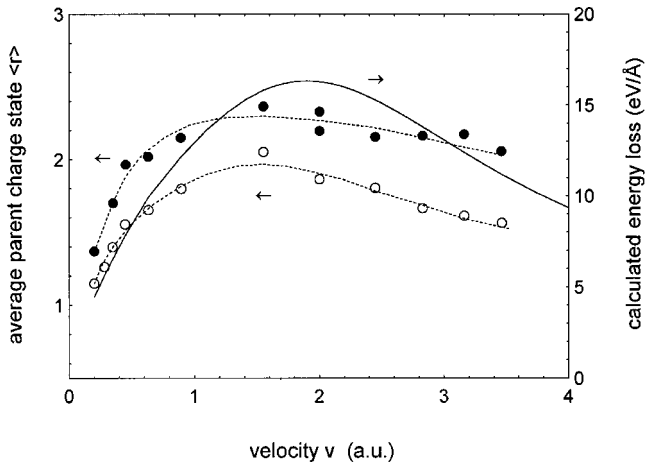

FIG. 11. Average charge state $\langle r \rangle$ of the parent fullerene ion before fragmentation (cf. text) as a function of the projectile velocity (open circles, including all impact parameters; full dots, penetrating collisions; the short-dashed lines are to guide the eye). The full curve indicates the velocity dependence of the electronic stopping power calculated with the TRIM code (right-hand scale).

grated for all m values ($m=0,1,\ldots$). The obtained values have been corrected for the detection efficiency assuming that at the highest postacceleration voltage (30 kV) all charge states are detected with the same probability. For lower acceleration voltages, correction factors are determined by comparing spectra measured at the same collision energy. The results, normalized with respect to the intensity for $r=1$, are shown in Fig. 10. When the collision energy is increased from 1 to 20 keV [see Fig. 10 (left figure)], the contributions from higher charge states become more important. It should be noted that the intensity of these charge states might even be underestimated since losses due to the emission of small charged fragments occur for $r \geqslant 3$, which lower the charge state of the detected residual ion. At energies above 60 keV, the probability for multi-ionization decreases and single ionization becomes more dominant [see Fig. 10(b)]. In order to represent the results in a single curve, we have defined an average charge state before fragmentation as $\langle r \rangle = \Sigma_r [rI(r)]/\Sigma_r I(r)$. Here $I(r)$ denotes the intensity of fullerene ions in the parent charge state r. It should be noted that this average value does not contain contributions from neutral fullerenes and, therefore, will show the tendency to approach the value $\langle r \rangle = 1$ for zero or very high velocities. In a similar way, an average charge $\langle r \rangle_h$ can be determined for penetrating collisions, replacing $I(r)$ by the intensity of the modeled ''hot'' component for a given charge state r.

In Fig. 11 we compare the average C_{60} charge before fragmentation, $\langle r \rangle$ and $\langle r \rangle_h$, with the relative electronic stopping power for H^+ in graphite as calculated with the TRIM code. The general behavior of all curves is similar, showing that ionization and electronic stopping power are closely related, which is in agreement with results presented in Refs. [9,20]. In the case of penetrating collisions, the average charge is slightly higher (0.5 units) than in the case when contributions from all impact parameters are taken into account.

VI. SUMMARY

We have studied collisions of hydrogen ions with fullerenes (C_{60}) in the energy range from 1 keV up to 300 keV, thus covering the velocity range from 0.2 to 3.5 a.u. The measured time-of-flight spectra yield information on the excitation, ionization, and multifragmentation of the produced fullerene ions.

In particular, we have discussed the role of electronic excitation and the transfer of electronic excitation energy into vibrational modes. Calculations with the aid of the TRIM code, as well as our Monte Carlo simulations, clearly show that in the present collision system the electronic interaction is by far dominant. An analysis of the evaporation signal (losses of C_2 dimers) and its dependence on the projectile velocity indicates that the vibrational excitation is due to a two-step mechanism. In a first step, energy is stored in the electronic system probably in the form of a multiplasmon excitation. In a second step, a part of this energy is transferred via the electron-phonon coupling into the heavy particle system. This finding is at variance with results obtained for He^+-C_{60} collisions, where a direct vibrational excitation has been found to be important [9]. It should be noted that in the latter case the nuclear stopping power becomes more important due to the higher projectile mass, and that for a given impact parameter with respect to a carbon atom a larger amount of energy will be transferred which may lead to a direct emission of a carbon atom. This direct emission will be less important in the hydrogen case. However, we assume that at larger velocities the electronic stopping power will contribute to the evaporation in the He case as well.

The intensity distributions of the evaporation sequence have been simulated within the evaporative ensemble model and vibrational energies have been estimated. At low energies these values compare reasonably well with the energy loss calculated within the Monte Carlo program and the TRIM code. This indicates that the electron-phonon coupling is a rather effective mechanism. At higher velocities, an appre-

ciable amount of the electronic energy loss stays in the electronic system, probably in the form of kinetic energy given to the emitted electrons.

The evaporation yield versus the TRIM-calculated electronic energy loss is found to be a double-valued function for velocities approaching one atomic unit. We have argued that this result is partly due to a difference in the ratio between the projectile energy loss and the amount of internal excitation energy, which is stored in the fullerene for low and high velocities. At low velocities, a large part of the electronic loss goes into internal excitation of the molecule, while some of the corresponding energy is spent as kinetic energy of the emitted electrons at higher velocities. This result confirms findings which are known from the interaction of ions with thin foils and DNA molecules.

ACKNOWLEDGMENTS

Part of the experiments has been performed at the Accélérateur d'Ions Multichargés (AIM), a facility of CEA-Grenoble. The authors would like to thank F. Gustavo for preparing the ion beam. We appreciate fruitful discussions with C. Guet, P. Hvelplund, and R. Moshammer. The Bielefeld group acknowledges the support of the Deutsche Forschungsgemeinschaft. The participation of the Stockholm group in this collaboration was founded by the Swedish Research Council.

[1] R. Deng, G. Littlefield, and O. Echt, Z. Phys. D: At., Mol. Clusters **40**, 355 (1997).
[2] N. Hay, E. Springer, M. B. Mason, J. W. G. Tisch, M. Castillejo, and J. P. Marangos, J. Phys. B **32**, L17 (1999).
[3] S. Hunsche, T. Starczewski, A. L'Huillier, A. Persson, C.-G. Wahlström, B. van Linden van den Heuwell, and S. Svanberg, Phys. Rev. Lett. **77**, 1966 (1996).
[4] G. F. Bertsch, A. Bulgac, D. Tomanek, and Y. Wang, Phys. Rev. Lett. **67**, 2690 (1991).
[5] M. Foltin, O. Echt, P. Scheier, B. Dünser, R. Wörgötter, D. Muigg, S. Matt, and T. D. Märk, J. Chem. Phys. **107**, 1 (1997).
[6] P. Scheier, B. Dünser, R. Wörgötter, D. Muigg, S. Matt, O. Echt, M. Foltin, and T. D. Märk, Phys. Rev. Lett. **77**, 2654 (1996).
[7] B. Dünser, O. Echt, P. Scheier, and T. D. Märk, Phys. Rev. Lett. **79**, 3861 (1997).
[8] E. E. B. Campbell, T. Raz, and R. D. Levine, Chem. Phys. Lett. **253**, 261 (1996).
[9] T. Schlathölter, O. Hadjar, R. Hoekstra, and R. Morgenstern, Phys. Rev. Lett. **82**, 73 (1999).
[10] A. Reinköster, U. Werner, and H. O. Lutz, Europhys. Lett. **43**, 653 (1998).
[11] B. Walch, C. L. Cocke, R. Voelpel, and E. Salzborn, Phys. Rev. Lett. **72**, 1439 (1994).
[12] T. LeBrun, H. G. Berry, S. Cheng, R. W. Dunfold, H. Esbensen, D. S. Gemmel, E. P. Kanter, and W. Bauer, Phys. Rev. Lett. **72**, 3965 (1994).
[13] N. Selberg, A. Barany, C. Biedermann, C. J. Setterlind, H. Cederquist, A. Langereis, M. O. Larsson, A. Wännström, and P. Hvelplund, Phys. Rev. A **53**, 874 (1996).
[14] Jian Jin, H. Khemliche, M. H. Prior, and Z. Xie, Phys. Rev. A **53**, 615 (1996).
[15] S. Martin, L. Chen, A. Denis, and J. Desesquelles, Phys. Rev. A **57**, 4518 (1998).
[16] S. Martin, L. Chen, A. Denis, and J. Desesquelles, Phys. Rev. A **59**, R1734 (1999).
[17] J. Opitz, H. Lebius, B. Saint, S. Jaquet, B. A. Huber, and H. Cederquist, Phys. Rev. A **59**, 3562 (1999).
[18] U. Thumm, T. Bastug, and B. Fricke, Phys. Rev. A **52**, 52 (1995).
[19] H. Cederquist, A. Fardi, K. Haghighat, A. Langereis, H. T. Schmidt, S. H. Schwartz, J. C. Levin, I. A. Sellin, H. Lebius, B. A. Huber, M. O. Larsson, and P. Hvelplund, Phys. Rev. A **61**, 022712 (2000).
[20] T. Schlathölter, O. Hadjar, J. Manske, R. Hoekstra, and R. Morgenstern, Int. J. Mass Spectrom. **192**, 245 (1999).
[21] H. Tsuchida, A. Itoh, K. Miyabe, Y. Bitoh, and N. Imanishi, J. Phys. B **32**, 5289 (1999).
[22] W. C. Wiley and I. H. McLaren, Rev. Sci. Instrum. **26**, 1150 (1955).
[23] F. Chandezon, B. A. Huber, and C. Ristori, Rev. Sci. Instrum. **65**, 3344 (1994).
[24] L. Plagne and C. Guet, Phys. Rev. A **59**, 4461 (1999).
[25] F. Aumayr, G. Betz, T. D. Märk, P. Scheier, and H. P. Winter, Int. J. Mass Spectrom. Ion Phys. **174**, 317 (1998).
[26] T. Bergen, X. Biquard, A. Brenac, F. Chandezon, B. A. Huber, D. Jalabert, H. Lebius, M. Maurel, E. Monnand, J. Opitz, A. Pesnelle, B. Pras, C. Ristori, and J. C. Rocco, Rev. Sci. Instrum. **70**, 3244 (1999).
[27] P. Moretto-Capelle, D. Bordenave-Montesquieu, and A. Bordenave-Montesquieu, Phys. Scr. **80**, 118 (1999).
[28] J. Becker, K. Beckord, U. Werner, and H. O. Lutz, Nucl. Instrum. Methods Phys. Res. A **337**, 409 (1994); U. Werner, J. Becker, T. Farr, and H. O. Lutz, Nucl. Instrum. Methods, Phys. Res. B **124**, 298 (1997).
[29] O. B. Firsov, Zh. Eksp. Teor. Fiz. **36**, 1517 (1959) [Sov. Phys. JETP **9**, 1076 (1959)].
[30] G. Moliere, Z. Naturforsch. A **2a**, 133 (1947).
[31] M. O. Larsson, P. Hvelplund, M. C. Larsen, H. Shen, H. Cederquist, and H. T. Schmidt, Int. J. Mass Spectrom. Ion Phys. **177**, 51 (1998).
[32] J. F. Ziegler, J. P. Biersack, and U. Littmark, *The Stopping and Range of Ions in Solids* (Pergamon, New York, 1985/1999.
[33] R. Wünsch, R. Neugebauer, T. Jalowy, D. Hofmann, H. Rothard, and K. O. Groeneveld, Nucl. Instrum. Methods, Phys. Res. B **146**, 82 (1998).
[34] G. Taucher-Scholz, J. Heilmann, and G. Kraft, Nucl. Instrum. Methods, Phys. Res. B **107**, 318 (1996).
[35] R. Katz, F. A. Cucinotta, and C. X. Zhang, Nucl. Instrum. Methods, Phys. Res. B **107**, 287 (1996).
[36] L. S. Kassel, J. Phys. Chem. **32**, 225 (1928).
[37] C. E. Klots, J. Phys. Chem. **92**, 5864 (1988); Z. Phys. D: At., Mol. Clusters **20**, 105 (1991).

[38] R. E. Stanton and M. D. Newton, J. Phys. Chem. **92**, 2141 (1988).
[39] M. Foltin, M. Lezius, P. Scheier, and T. D. Märk, J. Chem. Phys. **98**, 9624 (1993).
[40] K. Hansen and O. Echt, Phys. Rev. Lett. **78**, 2337 (1997).
[41] P. Hvelplund and B. Fastrup, Phys. Rev. **165**, 408 (1968).
[42] U. Saalmann and R. Schmidt, Phys. Rev. Lett. **80**, 3213 (1998); T. Kunert and R. Schmidt (unpublished).
[43] L. Plagne, Ph.D. thesis, Université Joseph Fourier de Grenoble I, Grenoble, France, 1998.